Electronic Supplementary Information (ESI) for

Sensitive Detection of Polycyclic Aromatic Hydrocarbons with Gold Colloid Coupled Chloride Ion SERS Sensor

Xuegang Gong, [a, b] Xiaoyong Liao, [a, *] You Li, [a] Hongying Cao, [a] Yishu Zhao, [a]

Haonan Li [a, b] and Daniel P. Cassidy [c]

a. Key Laboratory of Land Surface Pattern and Simulation, Beijing Key Laboratory of Environmental Damage Assessment and Remediation, Institute of Geographical Sciences and Natural Resources Research, Chinese Academy of Sciences, Beijing 100101, China

b. University of Chinese Academy of Sciences, Beijing 100049, China

c. Department of Geological & Environmental Sciences, Western Michigan University, Kalamazoo 49008, USA

*Address for correspondence. E-mail: liaoxy@igsnrr.ac.cn

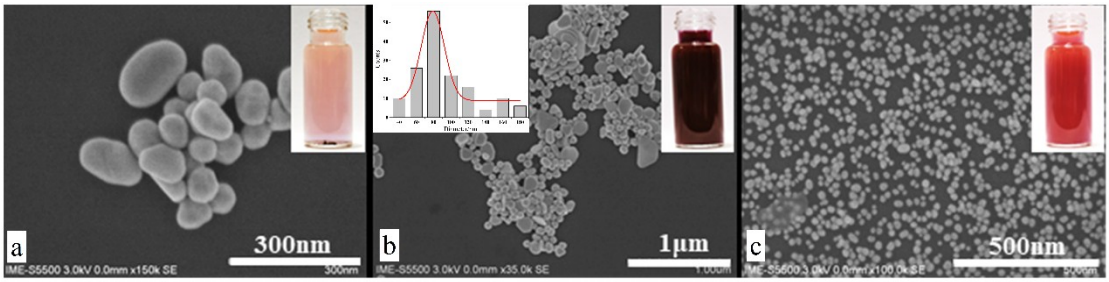

Fig. S1 SEM images of Au Nps with 1.0mL (a), 2.0 mL (b) and 3.5mL (c) of sodium citrate solution (1.0% wt). The inset photograph shows corresponding Au colloid.

Volume (Cl^-, 1M)	0 μL	80 μL	100 μL	120 μL	160 μL	200μL
Au colloid photograph	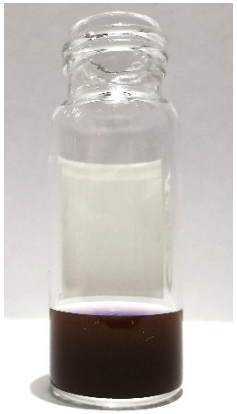	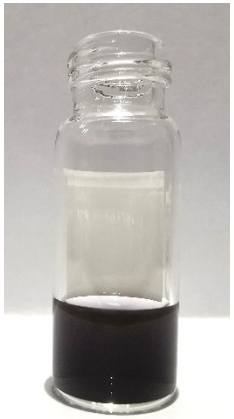				

Fig. S2 Photographs of Au colloid with different volumes of Cl^-(1M).

Table S1 The assignments of normal Raman and SERS bands of naphthalene (NaP), phenanthrene (PHE) and pyrene (PYR) [1-8].

Normal Raman Bands (cm^{-1})	SERS peaks (cm^{-1})			Assignment
	NaP	PHE	PYR	
408			405	skeletal stretching
409		403		skeletal stretching
511	507			skeletal stretching / C-C stretching
547		542		skeletal stretching
591			587	skeletal stretching
709		704		skeletal stretching
762	751			C-C stretching/ skeletal stretching
829		824		skeletal stretching
1020	1016			C-H in-plane bending / C-C stretching
1037		1028		C-C stretching/ HCC bending
1065			1055	C-H in-plane bending
1107			-	skeletal stretching
1142			-	C-H in-plane bending
1168	1158			C-C stretching/ C-H bending
1202		1200		C-C stretching/ HCC bending
1241			1231	C-C stretching/ C-H in-plane bending
1244		-		HCC bending
1349		1349		C-C stretching/ HCC bending
1381	1374			C-C stretching
1405			1398	C-C stretching/ ring stretching
1438		1427		C-C stretching/ HCC bending
1462	-			C-C stretching/ C-H bending
1523		-		C-C stretching
1574	1557			C-C stretching/ C-H in-plane bending
1593			-	C-C stretching
1612		1600		C-C stretching
1626			1607	C-C stretching

Section S1 DFT calculations for PAHs-Au_4 cluster

Quantum chemical calculations were performed with Gaussian 09 program package at the density function theory (DFT) level using B3LYP hybrid method. The 6-31G (d, p) basis set was selected for C, H atoms and LANL2DZ basis set for Au atom. In all computations, no constraints were imposed on geometry. The energy state analysis for HOMO and LUMO was carried out by GaussView software.

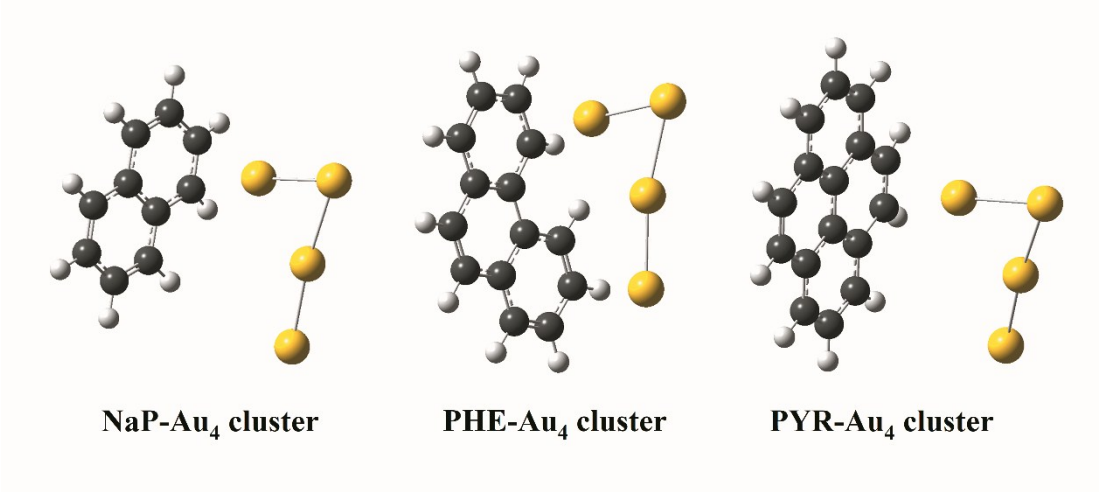

Fig. S3 The optimized molecular structures of PAH-Au_4 clusters.

Section S2 The calculation of EF (Enhancement factor) for PAHs.

The enhancement factors (EFs) was calculated by following equation [9,10]:

$$EF = \frac{I_{SERS}}{I_{Raman}} \times \frac{N_{Raman}}{N_{SERS}}$$

In this study, the I_{SERS} and I_{Raman} represent the signal intensities of the strongest Raman peaks of each PAH in SERS samples and the solid PAH, separately. N_{SERS} and N_{Raman} are the PAH molecule numbers that effectively excited by the laser beam in SERS sample solutions and solid PAH substance, respectively. Therefore, the N_{SERS} and N_{Raman} can be calculated with the following equations:

$$N_{SERS} = S_{laser} \cdot H_{solution} \cdot C_{PAH} \cdot N_A$$

$$N_{Raman} = \frac{S_{laser} \cdot H_{solid}}{M_{PAH}} \cdot \rho_{PAH} \cdot N_A$$

Thus, the equation of EF can also be translated into the following formula:

$$EF = \frac{I_{SERS}}{I_{Raman}} \times \frac{S_{laser} \cdot H_{solid} \cdot \rho_{PAH} \cdot N_A / M_{PAH}}{S_{laser} \cdot H_{\text{solution}} \cdot C_{PAH} \cdot N_A}$$

$$= \frac{I_{SERS}}{I_{Raman}} \times \frac{H_{solid} \cdot \rho_{PAH}}{H_{solution} \cdot C_{PAH} \cdot M_{PAH}}$$

S_{laser} is the effective circle area of laser spot with a diameter of 158 μm;

$H_{solution}$ is the depth of the incident laser beam in solution, here was about 2.2 mm;

H_{solid} is the penetration depth of the incident laser beam in solid PAH, about 20 μm;

C_{PAH} is the concentration of PAH in SERS sample solution, 1.72×10^{-7} mol·L^{-1};

N_A is the Avogadro constant, 6.02×10^{23} mol^{-1};

M_{PAH} is the molecular weight of solid PAH; g·mol^{-1};

ρ_{PAH} is the density of solid PAH; g·cm^{-3}.

Table S2 The set of concentrations for the three PAHs in quantitative detection experiments.

	Concentrations (μg/L)		
	NaP	PHE	PYR
a	0	0	0
b	2	1	1
c	5	2	2
d	10	5	5
e	20	10	10
f	40	20	20
g	80	40	40
h	100	80	80
i	200	100	100
g	400	200	200
k	600	400	400
l	800	600	600
m	1000	800	800
n	2000	1000	1000
o	4000	2000	2000
p	-	4000	4000

Note: *a* to *p* correspond to the letters in Fig. 5.

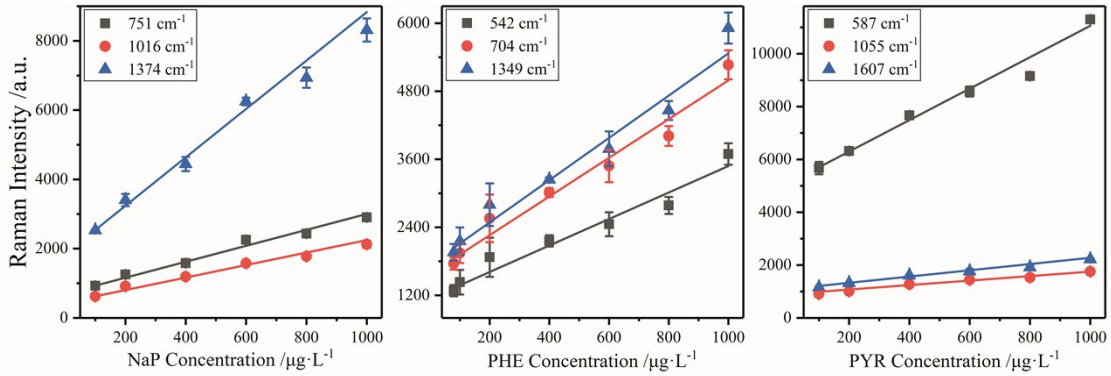

Fig. S4 The linear relationship for NaP (100-1000 μg/L), PHE (80-1000 μg/L) and PYR (100-1000 μg/L). The data points represent the average of three parallel samples. Data plotted as arithmetic mean with standard deviation error bars.

Table S3 The regression equations between Raman intensity and concentrations of NaP (100-1000 μg/L), PHE (80-1000 μg/L), and PYR (100-1000 μg/L).

PAH	Raman Peaks (cm^{-1})	Regression equation and correlation coefficient
NaP	751	$y = 701.21 + 2.30x$, $R^2 = 0.9908$
	1016	$y = 443.40 + 1.80x$, $R^2 = 0.9902$
	1374	$y = 1837.85 + 6.99x$, $R^2 = 0.9932$
PHE	542	$y = 1143.10 + 2.34x$, $R^2 = 0.9695$
	704	$y = 1576.94 + 3.41x$, $R^2 = 0.9764$
	1349	$y = 1740.00 + 23.73x$, $R^2 = 0.9736$
PYR	587	$y = 5107.65 + 5.95x$, $R^2 = 0.9798$
	1055	$y = 905.28 + 0.85x$, $R^2 = 0.9811$
	1607	$y = 1092.44 + 1.18x$, $R^2 = 0.9808$

Table S4 The calculated LOD (limit of detection) of PAHs.

PAH	Standard deviation	LOD (μg/L)	Raman peaks(cm^{-1})
NaP	11.58	1.38	1374
PHE	3.93	0.23	1349
PYR	8.16	0.45	587

The LOD was calculated with the following equation:

$$\mathrm{LOD} = \frac{3\sigma}{a}$$

Where σ is the standard deviation from the blank spectrum, *a* is the slope of linear correlation curves of the Raman intensities at discriminant peaks against concentrations for the three PAHs.

The standard deviations of the Raman intensities at the selected Raman peaks were listed in Table S4. The slope of the linear correlation curves at the selected Raman peaks were 25.16, 51.27 and 53.80, respectively.

Reference

1. Zhang, M.; Zhang, X.; Qu, B.; Zhan, J., Portable kit for high-throughput analysis of polycyclic aromatic hydrocarbons using surface enhanced Raman scattering after dispersive liquid-liquid microextraction. *Talanta* **2017,** *175*, 495-500.
2. Du, J.; Xu, J.; Sun, Z.; Jing, C., Au nanoparticles grafted on Fe3O4 as effective SERS substrates for label-free detection of the 16 EPA priority polycyclic aromatic hydrocarbons. *Anal. Chim. Acta.* **2016,** *915*, 81-89.
3. Shi, X.; Liu, S.; Han, X.; Ma, J.; Jiang, Y.; Yu, G., High-sensitivity surface-enhanced Raman scattering (SERS) substrate based on a gold colloid solution with a pH change for detection of trace-level polycyclic aromatic hydrocarbons in aqueous solution. *Appl. Spectrosc.* **2015,** *69*, (5), 574-579.
4. Wang, X.; Hao, W.; Zhang, H.; Pan, Y.; Kang, Y.; Zhang, X.; Zou, M.; Tong, P.; Du, Y., Analysis of polycyclic aromatic hydrocarbons in water with gold nanoparticles decorated hydrophobic porous polymer as surface-enhanced Raman spectroscopy substrate. *Spectrochim. Acta, pt. A Mol. Biomol. Spectrosc.* **2015,** *139*, 214-221.
5. Zhao, H.; Jin, J.; Tian, W.; Li, R.; Yu, Z.; Song, W.; Cong, Q.; Zhao, B.; Ozaki, Y., Three-dimensional superhydrophobic surface-enhanced Raman spectroscopy substrate for sensitive detection of pollutants in real environments. *J. Mater. Chem. A* **2015,** *3*, (8), 4330-4337.
6. Xu, J.; Du, J.; Jing, C.; Zhang, Y.; Cui, J., Facile detection of polycyclic aromatic hydrocarbons by a surface-enhanced Raman scattering sensor based on the Au coffee ring effect. *Acs Appl. Mater. Interface.* **2014,** *6*, (9), 6891-6897.
7. Gu, X.; Tian, S.; Zhou, Q.; Adkins, J.; Gu, Z.; Li, X.; Zheng, J., SERS detection of polycyclic aromatic hydrocarbons on a bowl-shaped silver cavity substrate. *Rsc Adv.* **2013,** *3*, (48), 25989-25996.
8. Kwon, Y.-H.; Sowoidnich, K.; Schmidt, H.; Kronfeldt, H.-D., Application of calixarene to high active surface-enhanced Raman scattering (SERS) substrates suitable for in situ detection of polycyclic aromatic hydrocarbons (PAHs) in seawater. *J. Raman Spectrosc.* **2012,** *43*, (8), 1003-1009.
9. Le Ru, E.; Blackie, E.; Meyer, M.; Etchegoin, P., Surface enhanced Raman scattering enhancement factors: a comprehensive study. *J. Phys. Chem. C* **2007,** *111*, (37), 13749-13803.
10. Hong, G.; Li, C.; Limin, Q., Facile fabrication of two-dimensionally ordered macroporous silver thin films and their application in molecular sensing. *Adv. Funct. Mater.* **2010,** *20*, (21), 3774-3783.